Journal of Neurochemistry

JOURNAL OF NEUROCHEMISTRY | 2015 | 133 | 330–342 doi: 10.1111/jnc.13001

ORIGINAL ARTICLE

Quantitative positron emission tomography of mGluR5 in rat brain with [^{18}F]PSS232 at minimal invasiveness and reduced model complexity

Adrienne Müller Herde,* Claudia Keller,* Selena Milicevic Sephton,* Linjing Mu,† Roger Schibli,*,† Simon M. Ametamey* and Stefanie D. Krämer*

*Center for Radiopharmaceutical Sciences ETH-PSI-USZ, Institute of Pharmaceutical Sciences, Department of Chemistry and Applied Biosciences (D-CHAB), ETH Zurich, Zurich, Switzerland

†Center for Radiopharmaceutical Sciences ETH-PSI-USZ, Department of Nuclear Medicine, University Hospital Zurich, Zurich, Switzerland

Abstract

Imaging the density of metabotropic glutamate receptor 5 (mGluR5) in brain by positron emission tomography (PET) is of interest in relation to several brain disorders. We have recently introduced [^{18}F]PSS232, an F-18-labeled analog of the mGluR5-targeting [^{11}C]ABP688. Quantitative PET requires kinetic modeling with an input function (IF) or an appropriate reference tissue model. We aimed at minimizing invasiveness of IF recording in rat and employing this protocol for mGluR5 quantitative PET with [^{18}F]PSS232. We further aimed at defining models of low complexity for quantitative PET with [^{18}F]PSS232. The IF was recorded in an arterio-venous shunt applied by minimally invasive cannulation. PET data were analyzed with a modified two-tissue compartment model including a single variable for radiometabolite correction in brain. We further evaluated a simple reference tissue model. Receptor-dependent accumulation was similar to [^{11}C]ABP688 at lower unspecific accumulation of unchanged [^{18}F]PSS232, in agreement with its higher plasma protein binding and lower lipophilicity. The minimally invasive protocol revealed similar results as the invasive shunt method and parameters calculated with the modified two-tissue compartment model were similar to those calculated with the standard model. The simple area under the curve ratios agreed with the Logan reference method. [^{18}F]PSS232 is a promising radioligand for mGluR5 quantification.

Keywords: area under the curve, cannulation, mGluR5, quantitative PET, radiometabolite, receptor imaging.

J. Neurochem. (2015) **133**, 330–342.

Cover Image *for this issue: doi: 10.1111/jnc.12875.*

Positron emission tomography (PET) with [^{11}C]ABP688 (Ametamey *et al.* 2006), targeting the allosteric binding site of the metabotropic glutamate receptor 5 (mGluR5), allowed to quantify alterations in human brain mGluR5 levels under various conditions (Deschwanden *et al.* 2011; Akkus *et al.* 2013; Hefti *et al.* 2013; Hulka *et al.* 2014; Martinez *et al.* 2014). We have recently introduced [^{18}F]PSS232, an ^{18}F-labeled analog of [^{11}C]ABP688 (Milicevic Sephton *et al.* 2013, 2015). The advantage of labeling with ^{18}F instead of ^{11}C is the increase in half-life of radioactive decay from 20 to 110 min. This allows distribution of the tracer to distant PET centers and to augment the number of PET scans per production at still high specific radioactivity (Bq/mol). This is of particular interest in preclinical research as it permits to increase group sizes and, therefore, statistical power. Because of its longer physical half-life, ease of radiosynthesis, acceptable extent of defluorination in rodents, and negligible defluorination with human liver microsomes (Milicevic Sephton *et al.* 2013, 2015), [^{18}F]PSS232 has the potential

Received September 18, 2014; revised manuscript received November 12, 2014; accepted November 21, 2014.

Address correspondence and reprint requests to Stefanie Krämer, Radiopharmaceutical Sciences, ETH Zurich, Vladimir-Prelog-Weg 4, CH-8093 Zurich, Switzerland. E-mail: stefanie.kraemer@pharma.ethz.ch

Abbreviations used: 1TCM, one-tissue compartment model; 2TCM, two-tissue compartment model; AV, arterio-venous; DVR, distribution volume ratio; MRT, mean residence time; PET, positron emission tomography.

to further mGluR5-related research and drug development in clinics and by small-animal PET.

Quantification of tracer accumulation is best achieved by kinetic modeling. Most information is gained from kinetic analysis involving an input function (IF), i.e., the radioactivity–time curve (TAC) of the parent tracer in the arterial plasma ($C_A(t)$). High temporal resolution of IF and PET data allows to determine the rate constants of individual processes. Kinetic modeling in neuroreceptor PET is generally based on a two-tissue compartment model (2TCM), including the IF, a first tissue compartment representing the free and non-specifically accumulated probe in the region of interest (ROI) and a second-tissue compartment for the receptor-associated probe. The simplest 2TCM assumes (pseudo-)first order (tracer concentration-independent) kinetics and reversibility in receptor binding. In this case, the kinetics depend on the IF and four parameters, defining the weighting function W (t): K_1 is a clearance term describing the passage of tracer from plasma into the first tissue compartment (volume/time per tissue cm^3), k_2 is the rate constant of the reverse transfer (1/time), and k_3 (pseudo-first order) and k_4 (first order) are the rate constants of receptor binding and dissociation (both 1/time), respectively. Radiometabolites that cross the blood–brain barrier contribute to the signal in the ROI. In the standard compartment models, this is taken into account by treating the radiometabolite as an additional tracer with its own IF (IF_m, $C_{A,m}(t)$) and weighting function $W_m(t)$ (Fujita *et al.* 1999). In the absence of specific binding in the ROI, radiometabolite kinetics follow a one-tissue compartment model (1TCM), defined by the IF_m and $K_{1,m}$ and $k_{2,m}$.

Equilibrium parameters such as binding potentials (BP), distribution volumes per cm^3 tissue (V), or distribution volume ratio (DVR) are determined by K_1 to k_4 as shown in eqns 1 to 6 (Innis *et al.* 2007). They are measures of the density of available binding sites (defined by k_3 and k_4), non-specific distribution of the tracer (defined by K_1 and k_2) or a combination thereof.

$$BP_P = V_S = K_1/k_2 \times k_3/k_4, \quad (1)$$

$$BP_{ND} = k_3/k_4, \quad (2)$$

$$V_S = BP_p = K_1/k_2 \times k_3/k_4, \quad (3)$$

$$V_T = K_1/k_2 \times (1 + k_3/k_4), \quad (4)$$

$$V_{ND} = K_1/k_2 \quad (5)$$

$$DVR = V_T/V_{ND}. \quad (6)$$

Indices $_P$, $_{ND}$, and $_S$ refer to parent tracer in plasma, non-displaceable tracer in tissue, and specifically bound tracer, respectively.

Recording of the blood TAC to generate the IF (and IF_m) is hampered by the invasiveness of standard protocols (Ingvar *et al.* 1991; Weber *et al.* 2002; Alf *et al.* 2013b). In addition, non-linear regression analysis with the 2TCM, in particular in the presence of radiometabolite(s) in the ROI, is often not reliable because of the high number of fitted variables (K_1 to k_4 for the parent tracer and $K_{1,m}$ and $k_{2,m}$ for each radiometabolite). Non-invasive reference tissue methods are, therefore, preferred to estimate equilibrium parameters. Tracer accumulation in the ROI is compared to its distribution to a reference region, ideally devoid of specific binding, assuming identical ratios K_1/k_2 (and $K_{1,m}/k_{2,m}$) in ROI and reference tissue (Ichise *et al.* 2001; Carson 2003). Equilibrium parameters can thus be estimated directly from the PET data of ROI and reference region (Logan *et al.* 1996; Ichise *et al.* 2001; Carson 2003). However, this includes an unknown bias as most methods are based on assumptions such as complete absence of specific binding in the reference region and equal tracer distribution in the reference region and the first tissue compartment of the ROI. In addition, some methods require the input of one or more parameters determined with the 2TCM (Logan *et al.* 1996; Ichise *et al.* 2001).

We recently applied a simple model- and IF-independent method to quantify [^{18}F]PSS232 accumulation in rat brain. We used the ratio of the areas under the TACs of ROI and reference region for quantification (area under the curve, AUC ratio method). The reference region was a 52 mm^3 sphere in the cerebellum (CBref), a brain region with negligible mGluR5 in rats (Elmenhorst *et al.* 2010; Milicevic Sephton *et al.* 2015). This method revealed inter-individual differences of < 10% for individual ROIs allowing quantitative PET at high statistical power.

In this work, we apply kinetic modeling with an IF to address the following issues related to neuroreceptor imaging in rats in general and quantitative PET with [^{18}F]PSS232 in particular. The first point we addressed was a technical issue of general interest in preclinical PET. Recording of an IF with high temporal resolution in rodents can best be achieved with an arterio-venous (AV) shunt (Weber *et al.* 2002; Alf *et al.* 2013b). Here, we show that surgery is not a prerequisite for the AV-shunt in rats. We tested a novel, minimally invasive cannulation protocol that we first optimized with [^{18}F]FDG and then applied for kinetic modeling with [^{18}F]PSS232. Second, we analyzed the kinetics of [^{18}F]PSS232 and its radiometabolite in rat brain with the 2TCM extended by $K_{1,m}$ and $k_{2,m}$. We furthermore introduce a method (modified 2TCM, m2TCM) to correct for radiometabolite(s) in the ROI by extending the 2TCM by a single variable k_m, reducing the number of variables from six to five. Third, we validated the simple model-independent AUC ratio method for [^{18}F]PSS232 and finally applied this method to investigate whether the pre-scan interventions required for the AV-shunt affect quantitative PET with [^{18}F]PSS232. The m2TCM and AUC ratio method are described below in greater detail.

The modified 2TCM (m2TCM)

The standard 2TCM and our m2TCM are schematically shown in Figure S1. While the number of radiometabolites distributing to the brain does not need to be specified in the m2TCM, here it is assumed one for the 2TCM. Equation 7 shows the function that describes the TAC of a ROI ($C_{ROI}(t)$ in Bq per tissue volume) after correction for the contribution of whole blood radioactivity ($C_{wb}(t)$) and fractional vascular space (v_b), resulting in $C_{ROI,T}(t)$, the tracer radioactivity in ROI tissue.

$$[C_{ROI}(t) - v_b \times C_{wb}(t)]/(1 - v_b) = C_{ROI,T}(t) = [C_A(t) \otimes W + C_{A,m}(t) \otimes W_m], \quad (7)$$

W of the 2TCM is a biexponential function as shown in eqn 8 where base values and rate constants are composites of K_1 to k_4 (Ichise *et al.* 2001). Assuming a 1TCM for the radiometabolite, W_m equals $K_{1,m} \times \exp(-k_{2,m} \times t)$ (Ichise *et al.* 2001). Equation 7 can be solved for the six parameters K_1, k_2, k_3, k_4, $K_{1,m}$, and $k_{2,m}$ by non-linear regression analysis.

$$W = \phi_1 \times \exp(-\theta_1 \times t) + \phi_2 \times \exp(-\theta_2 \times t). \quad (8)$$

The high number of variables in eqn 7 often reveals unreliable fits, depending on the quality of TAC and IF data (Fujita *et al.* 1999). We, therefore, evaluated a simplified model for PET kinetic modeling with [^{18}F]PSS232 to correct for radiometabolite(s) in the ROI, reducing the number of variables to five. In the case of [^{18}F]PSS232, the ratio of parent to total radioactivity in rat brain followed an exponential function with the rate constant $k_{m,brain}$, as concluded from the analysis of brain homogenate at various time points after tracer injection. $C_{brain,T}(t)$ may thus be corrected for the contribution of radiometabolite according to eqn 9.

$$C_{parent,brain,T}(t) = C_{brain,T}(t) \times \exp(-k_{m,brain} \times t). \quad (9)$$

Depending on the ratio of specifically bound tracer to total radioactivity, $k_{m,brain}$ may vary between brain regions in addition to the inter-individual variability. We, therefore, included k_m in the fit function as shown in eqn 10, with a variable $k_{m,ROI}$ instead of the experimentally determined $k_{m,brain}$.

$$C_{ROI,T}(t) = (C_A(t) \otimes W)/\exp(-k_{m,ROI} \times t) = (C_A(t) \otimes W) \times \exp(k_{m,ROI} \times t). \quad (10)$$

Equation 10 can be solved for the five variables K_1, k_2, k_3, k_4, and $k_{m,ROI}$. In theory, any alternative function other than an exponential can be applied for radiometabolite correction in the ROI. The kind of function needs to be determined experimentally once while the parameters for individual animals and brain regions are fitted. This method may be of particular interest if more than one radiometabolite contributes to the signal in the ROI, if all plasma radiometabolites do not distribute to the brain or if one or more radiometabolite(s) is formed in brain. Under these conditions, the standard 2TCM according to eqn 7 may fail. As for radiometabolite correction with a 1TCM, the method is only applicable if the kinetics in the brain of radiometabolite(s) and parent tracer differ substantially.

The AUC ratio reference tissue method

AUC is a model-independent parameter easily estimated from $C_{ROI}(t)$ by the trapezoidal rule ($\Sigma(C_{ROI}(t_i) \times$ (duration of time interval i))). As the IF is equal for the ROI and the reference region, the ratio of the AUCs of the ROI and reference region, determined from $t = 0$ to $t = \infty$ equals the ratio of the respective integrated W, i.e., $V_{T,ROI}/V_{T,Reference}$ (Logan *et al.* 1996). At t_n (last time point) $< \infty$, the AUCs of the ROI and reference region need to be expanded by the respective $C_{ROI}(t_n)$ multiplied with the mean residence time (MRT) of the tracer in the respective tissue at t_n. This equals $C_{Reference}(t_n) \times 1/k_{2,Reference}$ for the reference region (Logan *et al.* 1996) and approximately $C_{ROI}(t_n) \times 1/\theta_2$ for the ROI, where θ_2 is the apparent rate constant of the terminal phase of W [eqns 8, 11 and (Ichise *et al.* 2001)].

$$\theta_2 = 1/2 \times [k_2 + k_3 + k_4 - ((k_2 + k_3 + k_4)^2 - 4 \times k_2 \times k_4)^{0.5}]. \quad (11)$$

Both terms $C(t_n) \times$MRT become negligible at scan durations, where $C(t_n)$ of ROI and reference region are low compared to earlier time points and t_n is substantially longer than $1/k_2$ and $1/\theta_2$. Under these conditions, the AUC ratio of ROI and reference region becomes constant and any correction for an intercept in the Logan reference tissue plot becomes negligible with the result that the AUC ratio directly equals the slope determined in the Logan reference tissue plot and t^* in the Logan reference tissue plot can be set to 0 (Logan *et al.* 1996). $V_{T,ROI}/V_{T,Reference}$ equals DVR in case $V_{T,Reference}$ equals V_{ND} (eqn 6).

Taking into account a radiometabolite with no specific binding, the AUC ratio under above conditions should become smaller than $V_{T,ROI}/V_{T,Reference}$ as the relative contribution of radiometabolite is higher in the reference region than in the ROI where parent tracer alone distributes to the second tissue compartment in addition to the first. The error is expected equal for the slope of the Logan reference tissue plot and the AUC ratio.

Material and methods

Animals

Animal husbandry and experiments were in accordance with the Swiss legislation on animal welfare and were approved by the Veterinary Office of the Canton Zurich, Switzerland. If not stated otherwise, male wild-type (WT) Wistar rats from Charles River (Sulzfeld, Germany) were used. Male mGluR5 knockout (KO) rats (SD-Grm5^{tm1sage}, on a Sprague–Dawley background) and male Sprague–Dawley control WT rats were purchased from SAGE labs Inc. (Boyertown, PA, USA). Animals were allowed to adapt for at least 1 week at a 12/12-h light/dark cycle and normal chow.

Ex vivo biodistribution

Four awake mGluR5 KO rats (206–242 g) and four awake control Sprague–Dawley WT rats (239–279 g) received into a tail vein 4.5–8.6 MBq (0.17–0.29 nmol/kg) [^{18}F]PSS232, synthesized as previously described (Milicevic Sephton *et al.* 2013). After 42 min, rats were anesthetized with isoflurane in air/oxygen and killed by decapitation 45 min after tracer injection. Brains were dissected and radioactivity determined in the indicated brain regions with a gamma counter (1480 Wizard 3", Perkin Elmer). Specific binding was calculated according to eqn 12. $C_{Reference}$ was either the average radioactivity per g tissue of the respective ROI of the mGluR5 KO rats or cerebellum of the individual WT rat.

$$\%\,\text{Specific binding} = (C_{ROI} - C_{Reference})/C_{ROI} \times 100\,\%. \quad (12)$$

Ratio of parent tracer to total radioactivity in plasma and brain

Eight rats (225–353 g) were injected into a tail vein under isoflurane anesthesia with 200–450 MBq (< 10 nmol/kg) [^{18}F]PSS232. Ratios of parent tracer to total radioactivity in plasma and brain were determined by radio-TLC as described in the Supporting Information (Milicevic Sephton *et al.* 2013, 2015) and were fitted with a monoexponential function as shown in eqn 13.

$$r_{parent/total}(t) = [1 - r_{parent/total}(t = \infty)] \times \exp(-k_m \times t) + r_{parent/total}(t = \infty). \quad (13)$$

Blood cell partitioning and free (unbound) fraction in plasma (f_u) were determined by blood cell separation and equilibrium dialysis, respectively, as described in the Supporting Information.

Arterio-venous shunt

An AV-shunt was applied either by surgery or by direct cannulation (minimally invasive protocol). For both protocols, animals were anesthetized with ca 2.5% isoflurane in oxygen/air 1 : 1 on a heating pad (Harvard Apparatus, Holliston, Massachusetts, USA) at 37°C. Surgery was performed as described previously (Weber *et al.* 2002; Alf *et al.* 2013b). In brief, the right femoral artery and vein were dissected and heparinized polyethylene catheters (neoLab-PE Micro-tubing 0.58 × 0.96 mm, Wiegand International, Hamburg, Germany) were introduced to artery and vein and connected via a three-way valve a few cm away from the venous entry. For the cannulation protocol, the tail was heated in a water bath and the heparinized catheters manually connected to needles G21 were inserted into the artery and a lateral vein of the tail, respectively. The tail was heated throughout the scan as indicated below. For both protocols, the shunt was guided through the coincidence counter twilite (swiss*trace*, Zurich, Switzerland) and a peristaltic pump (Ismatec, Glattbrugg, Switzerland) providing a blood flow of 200–300 μL/min. Counter and pump were positioned as close as possible to the bed of the PET/CT scanner to reduce catheter lengths and the pump was started as soon as the animal was positioned. Blood coincidences were recorded with the software PMOD (PMOD, Zurich, Switzerland). Control experiments revealed no detectable adsorption of [^{18}F]PSS232 to the catheter in the presence of plasma protein (data not shown).

PET scans and time–activity curves

PET scans were performed with a calibrated VISTA eXplore (Argus) PET/CT scanner (Sedecal, Madrid, Spain). Respiratory rate and temperature were controlled as previously described (Alf *et al.* 2013b). [^{18}F]FDG from clinical production (University Hospital Zurich, Switzerland) or [^{18}F]PSS232 was infused over 6–13 s in the free (non-cannulated) tail vein at doses between 14 and 39 MBq [^{18}F]FDG (350–400 μL) or between 24 and 42 MBq (0.6 and 6 nmol/kg) [^{18}F]PSS232 in 350–600 μL ethanol/water/PEG200 (5 : 47.5 : 47.5). In total, 19 rats were scanned: two mGluR5 KO and two Sprague–Dawley WT control rats with [^{18}F]PSS232, without AV-shunt, four rats with surgery and four rats with cannulation with [^{18}F]FDG, and four rats with surgery and five rats with cannulation with [^{18}F]PSS232. The blood coincidence counter was started 30–40 s before tracer infusion to record the background signal. Tracer infusion and dynamic PET acquisition (list mode) were started simultaneously and PET scans and blood counting were run for 90 min. To exclude binding of [^{18}F]PSS232 to any alternative target than mGluR5, one KO animal was injected intravenously 40 min after the tracer with 1 mg/kg unlabeled PSS232 to displace the tracer from any potential alternative target. At the end of each scan, a CT was recorded for anatomical orientation. Rats with surgery were killed after the scan while rats without or with minimally invasive shunt were allowed to wake up. PET data were reconstructed and TACs ($C_{ROI}(t)$ in Bq/cm^3) of brain regions calculated with PMOD, respectively, as described in the Supporting Information and Figure S2.

Estimation of spillover

Radioactivity spillover from skull was estimated from the two scanned mGluR5 KO rats. We assumed zero spillover in thalamus, the brain region with lowest signal in the mGluR5 KO rats. The TACs of an mGluR5 KO rat are shown in Figure S3. Spillover from skull to individual ROIs ($f_{spillover,ROI}(t)$) was calculated as shown in eqn 14. For spillover correction, the $f_{spillover,ROI}(t)$ values from 60 to 90 min of the two mGluR5 KO rats were averaged ($f_{spillover,ROI}$). The $f_{spillover,ROI}$ values ranged from 0.026 for midbrain to 0.28 for cortex (Table S1).

$$f_{spillover,ROI}(t) = [C_{ROI}(t) - C_{thalamus}(t)]/[C_{skull}(t) - C_{thalamus}(t)]. \quad (14)$$

Input function

Blood coincidences were corrected for the background counts and the time point $t = 0$ before radioactivity started to increase was

defined by visual inspection. Coincidences were further corrected for radioactive decay and according to the calibration factor between PET and coincidence counter to reveal decay-corrected whole-blood radioactivity per cm^3 ($C_{wb}(t)$) (Alf *et al.* 2013b). $C_{wb}(t)$ was transformed to plasma radioactivity per cm^3 ($C_{plasma}(t)$) by multiplying $C_{wb}(t)$ with 1/(1-Ht), where Ht is the hematocrit, i.e., 0.44 (Susic *et al.* 1984; Boylan *et al.* 1991). $C_{plasma}(t)$ was further corrected for $r_{parent/total}(t)$ to result in the radioactivity of parent tracer per cm^3 plasma, $C_A(t)$, the IF (eqn 15).

$$C_A(t) = C_{wb}(t)/(1 - Ht) \times [(1 - r_{parent/total}(t = \infty)) \times \exp(-k_{m,plasma} \times t) + r_{parent/total}(t = \infty)]. \quad (15)$$

Kinetic modeling with input function

Kinetic modeling of [^{18}F]PSS232 was performed blinded with a home-written MATLAB code (MathWorks) (Supporting Information) and PMOD. TACs of individual ROIs were first corrected for radioactivity spillover from skull according to eqn 16.

$$C_{ROI,spillover-corr}(t) = C_{ROI}(t) - f_{spillover,ROI} \times [C_{skull}(t) - C_{CBref}(t)]. \quad (16)$$

Negative values for [$C_{skull}(t)$-$C_{CBref}(t)$] at early time points were set to 0. Next, $C_{ROI,spillover-corr}(t)$ was further corrected for radioactivity contribution of blood and for fractional blood volume in tissue (v_b) as shown in eqn 17

$$C_{ROI,T}(t) = [C_{ROI,spillover-corr}(t) - v_b \times C_{wb,fit}(t)]/(1 - v_b), \quad (17)$$

where $C_{wb,fit}(t)$ is the blood radioactivity at time t as calculated from a three-exponential fit of the blood curve as described previously (Alf *et al.* 2013a). A value of 0.05 was assumed for v_b for all brain regions (Backes *et al.* 2011).

Kinetic parameters were next fitted with the 2TCM and the m2TCM, respectively, according to eqns 7 and 11, by iterative least squares estimation with MATLAB. Equilibrium parameters were calculated from the fit parameters as shown in the Introduction (eqns 1–6) (Innis *et al.* 2007). Weighting factor was $1/C_{ROI,T}(t)$ if not stated otherwise. To evaluate the influence of the radiometabolite on the experimental TAC, $C_{ROI,T}(t)$ were corrected with the fitted $k_{m,ROI}$ to get the respective TAC of the parent tracer as shown in eqn 18. Finally, radioactivity of the parent tracer in the first ($C_{parent,ROI,TC1}$) and second tissue compartments ($C_{parent,ROI,TC2}$) were simulated according to the MATLAB code in the Supporting Information (W1_comp1, W1_comp2, mW1_comp1, mW1_comp2).

$$C_{parent,ROI}(t) = C_{ROI,T}(t) \times \exp(-k_{m,ROI} \times t), \quad (18)$$

Kinetic modeling without an input function

Specific binding was estimated blinded as AUC_{ROI}/AUC_{CBref} with AUCs from 0 to 75 min. This time window was chosen to allow for the direct comparison with our recently published data (Milicevic Sephton *et al.* 2013, 2015). TACs were furthermore analyzed with the Logan reference tissue method with PMOD with CBref as reference tissue (Logan *et al.* 1996). Most t^* values were < 10 min (two at 12.5 min) and $k_{2,CBref}$ was fixed at 5 (1/min), as estimated with the 2TCM and m2TCM (Table S2). Both reference tissue models were without any correction for spillover or radiometabolite.

Statistical analysis

Average values are shown with their SD. Parameters were compared by Student's t-test and in Bland–Altman plots. *t*-tests were homoscedastic and unpaired (two-sample analysis), unless stated otherwise. A value of $p < 0.05$ was considered significant.

Results

Specificity and selectivity of PSS232 to rat mGluR5

To confirm specificity and selectivity for mGluR5 *in vivo* in rats, we compared [^{18}F]PSS232 accumulation in brain of mGluR5 KO and WT rats by PET and in an *ex vivo* biodistribution experiment. Figure 1 shows the respective PET images averaged from 2 to 60 min. TACs of a WT rat are shown elsewhere (Milicevic Sephton *et al.* 2013, 2015), TACs of a KO rat are shown in Figure S3. No accumulation was found in brain of the KO rats. Application of excess PSS232 did not further reduce radioactivity in any brain region of a KO rat, excluding detectable binding to an alternative target (data not shown). The results of the *ex vivo* biodistribution experiment are shown in Fig. 1(c). WT rats had significantly ($p < 0.01$) higher normalized radioactivity (in Bq per g tissue, normalized to the injected radioactivity in Bq per g body weight, corresponding to the standardized uptake value SUV) in all brain regions than KO rats, with the exception of cerebellum. Normalized radioactivity in all brain regions of the KO rats was similar as in cerebellum of both WT and KO rats with no significant difference. The radioactivity (Bq/g) ratio between striatum and cerebellum of the WT rats was, on average, 4.60 ± 0.31. Normalized radioactivity in striatum of WT rats was, on average, (4.32 ± 0.43)-fold higher than the averaged normalized radioactivity in striatum of KO rats. The two ratios were not significantly different and correspond to 78.3 and 76.8% specific binding, respectively, in agreement with the 78.5% displaceable binding that we recently extrapolated in a displacement experiment with increasing doses of the mGluR5 antagonist MMPEP (Milicevic Sephton *et al.* 2013, 2015).

Evaluation of the minimally invasive AV-shunt method

We first optimized our minimally invasive protocol for the recording of the IF with [^{18}F]FDG. We started with eight rats (348–404 g), four for each protocol. Recording of IF and PET data was successful with all four rats with surgery. With the cannulation protocol, blood clocked in the shunts of the first two animals during the scan. For the third and fourth animals with the cannulation protocol, we heated the tail on a heating pad (37°C) during the PET scan. This allowed continuous blood flow through the coincidence counter

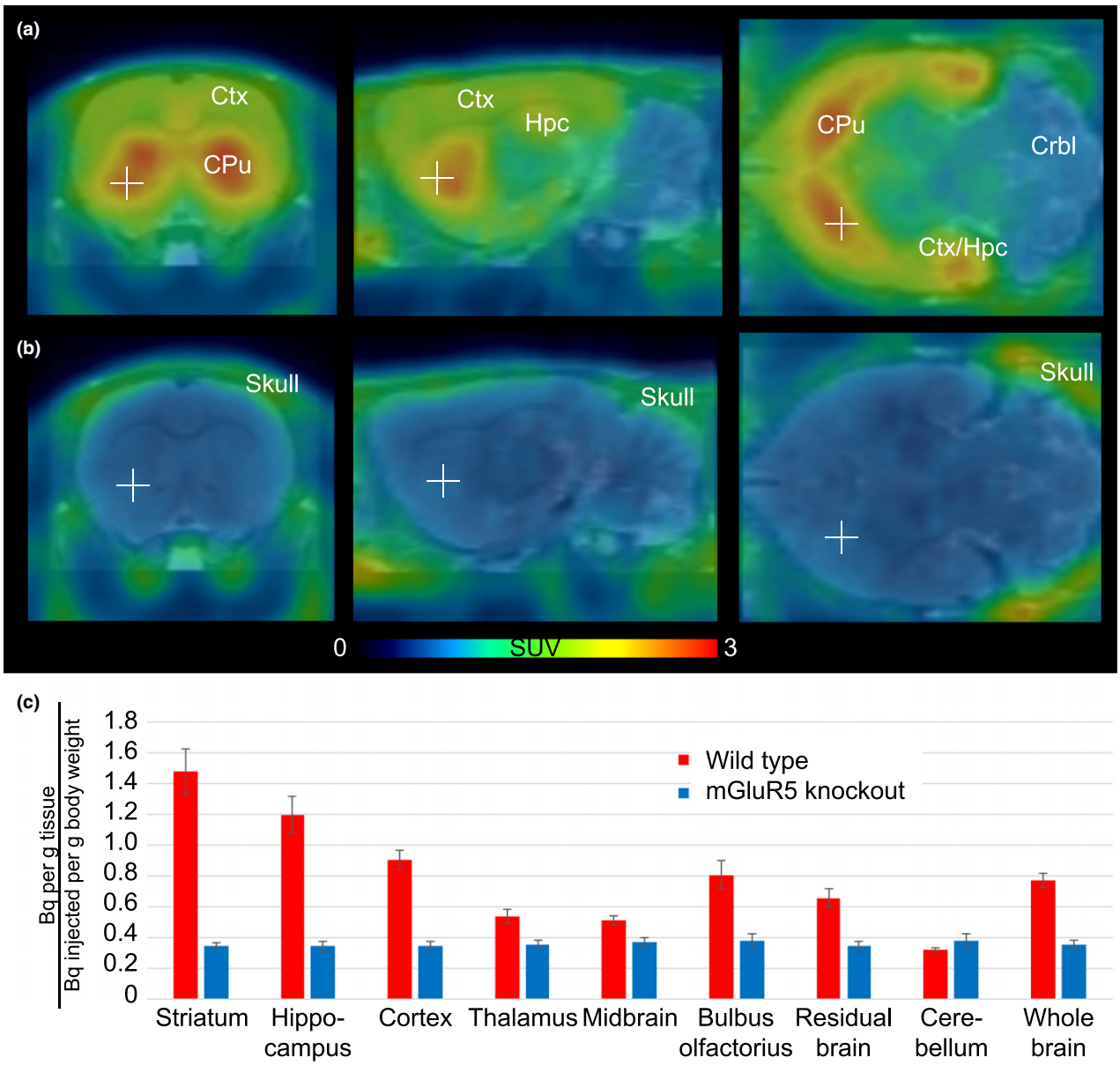

Fig. 1 Positron emission tomography (PET) images and *ex vivo* biodistribution of [18F]PSS232 in brains of WT and metabotropic glutamate receptor 5 (mGluR5)-KO rats. (a and b) 37 MBq (1.5 nmol/kg) [18F]PSS232 was applied intravenously to a 193 g weighing WT rat (a) and 37 MBq (0.8 nmol/kg) to a 169 g weighing mGluR5 KO rat (b). PET data were averaged from 2 to 60 min after tracer injection and matched to an MRI template (PMOD). (c) *Ex vivo* biodistribution after intravenous injection of 4.5–8.6 MBq (0.17–0.29 nmol/kg) [18F]PSS232. Average values with SD, $n = 4$ for each group. Differences between WT and mGluR5 KO rats were significant, except for cerebellum. Ctx, cortex; CPu, striatum; Hpc, hippocampus; Crbl, cerebellum. SUV, standardized uptake value (Bq per cm^3/Bq injected dose per g body weight). Cross hairs indicate image planes.

during the complete scan duration of 90 min. Anesthesia duration before scan start was about 30–60 min for the surgery protocol and 15–30 min for the cannulation protocol. The fit parameters for FDG are shown in Figure S4.

Proceeding with [18F]PSS232, three of the five rats (381–422 g) with minimally invasive AV-shunt were finally used for data analysis. One of the remaining two moved its head during the scan, the other one was excluded as the blood TAC had an unrealistic shape. Anesthesia durations before scan start were 45–90 min for the surgery and 30–45 min for the cannulation protocol, including some idle time before tracer delivery. The blood TACs of [18F]PSS232 as recorded with both AV-shunt protocols are shown in Fig. 2.

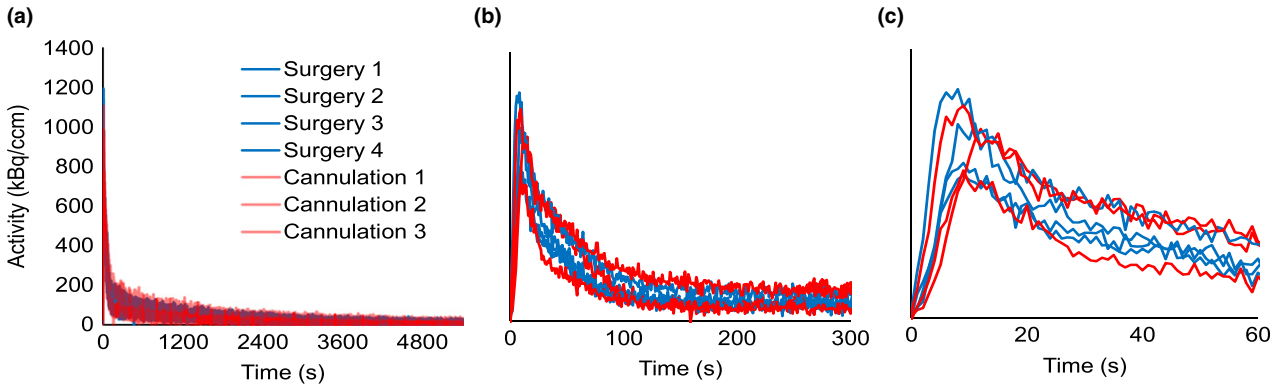

Fig. 2 Blood TACs of [^{18}F]PSS232 in rats recorded with an invasive and a minimally invasive arterio-venous (AV)-shunt protocol. Shunt from femoral artery to femoral vein applied by surgery (blue); shunt by direct cannulation of tail artery and vein (red). Infusion durations between 6 and 13 s. (a) Complete blood TAC; (b) first 5 min; (c) first min.

Characterization of the radioactivity in plasma and brain and generation of the [^{18}F]PSS232 input function

The plasma fraction contained (80.6 ± 5.6) % of total radioactivity after 5- to 90-min incubation of rat blood with [^{18}F]PSS232 *in vitro*. The free fraction f_u in rat and human plasma was 0.03 (± 0.000 and ± 0.001, respectively). Both blood cell partitioning and plasma protein binding were not taken into account to generate the IF. Figure 3 shows the kinetics of parent tracer to total radioactivity in plasma and brain after intravenous tracer application. Parent/total radioactivity ratios $r_{parent/total}(t)$ in plasma and brain followed exponential functions (eqn 13) with $r_{parent/total}(t = \infty)$ 0.14 for plasma and 0 for brain and k_m (1/min) 0.035 for plasma and 0.0060 for brain. The IF ($C_A(t)$) was calculated from the blood TAC as shown in eqn 15, IF_M was calculated as the difference between $C_{plasma}(t)$ and $C_A(t)$. Figure 3 shows a typical blood radioactivity curve with the corresponding IF (AV-shunt by surgery).

Kinetic modeling with [^{18}F]PSS232

TACs of brain regions were corrected as described under Methods for spillover from skull, contribution of whole blood, and for vascular space and were analyzed with the 2TCM including correction with a 1TCM for a radiometabolite and with the m2TCM. Typical TACs of striatum, whole brain, and CBref with the respective fits are shown in Fig. 4 (same rat as in Fig. 3b). Averaged fit and respective equilibrium parameters are shown in Fig. 5 and Table S2. None of the ROIs followed a 1TCM as shown for striatum and CBref in Figure S5.

The receptor-dependent parameters BP_P, BP_{ND}, V_T, and DVR but not the receptor-independent V_{ND} were significantly different between CBref and the mGluR5-rich regions striatum, hippocampus, cingulate cortex, cortex as well as whole brain, independent of the shunt and calculation methods (Table S2). Significances comparing the ROIs with whole brain are indicated in Fig. 5. None of the parameters showed any dose dependence (data not shown).

Parameters calculated with the 2TCM and the m2TCM were not significantly different applying an unpaired t-test. Applying a paired *t*-test, k_4 of most brain regions after the surgery protocol (thalamus after the cannulation protocol) differed between the two models. Average k_4 values were between 5 and 27% higher when estimated with the m2TCM

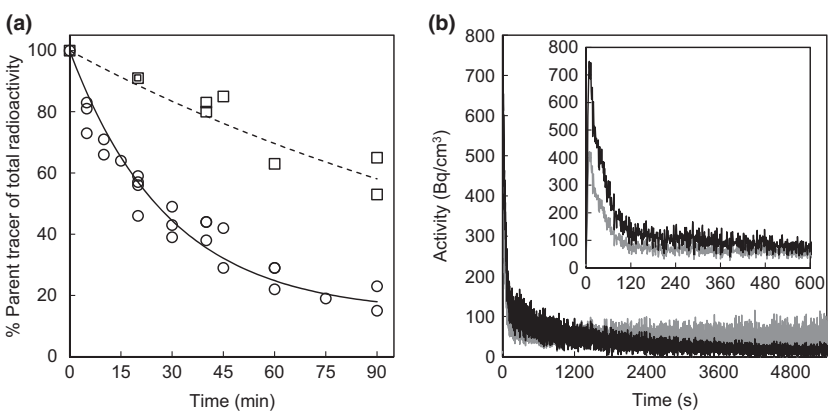

Fig. 3 [^{18}F]PSS232 parent tracer and total radioactivity in plasma and brain. (a) % Parent tracer of total radioactivity in plasma (circles) and brain (squares) was fitted to exponential functions (lines, fit parameters see text). (b) Whole blood curve (gray) and calculated IF (black) after intravenous administration of 23.9 MBq (0.7 nmol/kg) [^{18}F]PSS232 over 9 s to a 437 g rat. The insert shows first 10 min after injection.

than with the 2TCM. Equilibrium parameters were not different comparing the 2TCM and m2TCM analysis with an unpaired t-test but differed when applying a paired *t*-test. Figure S6 shows the respective Bland–Altman plots for striatum and brain. For all parameters, zero difference was included in the 95% confidence intervals of the differences between the two calculation methods. A significant bias (mean difference significantly different from 0, $p < 0.05$) was observed for k_4 (10% higher values for m2TCM) and k_4-dependent equilibrium parameters. The sum of the squared residuals were 0.27% and 0.93% higher for the m2TCM than the standard 2TCM for striatum and brain, respectively, of the scan shown in Fig. 4.

Comparing the invasive and minimally invasive AV-shunt protocols, none of the constants K_1 to k_4 or equilibrium constants was significantly different between the two methods, except of one value indicated with # in Fig. 5. The fitted $k_{m,ROI}$ was, on average, (1.5 ± 0.07)-fold higher in the cannulation group. Average $V_{ND,m}$ and $k_{m,ROI}$ values are shown in Figure S7. As expected based on the higher number of variables in the 2TCM than in the m2TCM, variations of $K_{1,m}$ and $k_{2,m}$ were substantially higher than of $k_{m,ROI}$ (Table S2).

The influence of $k_{m,ROI}$ (1/min) on kinetic modeling was investigated with the data set shown in Figs 3(b) and 4 (fitted $k_{m,striatum}$ 0.0093 and $k_{m,CBref}$ 0.013). When $k_{m,ROI}$ was kept fixed at 0.006 as determined from brain homogenates (Fig. 3a), K_1 to k_4 of striatum were reduced by 3.3, 15, 24, and 19%, respectively. Changes in BP_P, BP_{ND}, V_T, DVR, and V_{ND} did not exceed 10%. Neglecting correction ($k_{m,striatum} = 0$) did further reduce K_1 to k_4. V_T and V_{ND} of striatum were 20 and 27% higher, respectively, than after including $k_{m,ROI}$ in the fit. Changes in BP_{ND} and DVR were < 7%. Results and residuals for the three fits with fitted, fixed, or neglected k_m are shown in Figure S8.

We further evaluated the influence of spillover from skull on the analysis with the data set shown in Figs 3(b) and 4. The parameters correcting for the radiometabolite, i.e., $K_{1,m}$, $k_{2,m}$, or $k_{m,ROI}$ compensated for a missing spillover correction. For striatum, $V_{ND,m}$ and $k_{m,striatum}$ were increased by 6 and 5%, respectively, while all other parameters differed by less than 1% from the analysis with spillover correction. For cortex, which was most affected by spillover from skull, $V_{ND,m}$ and $k_{m,striatum}$ increased by 57 and 36%, respectively, to compensate for spillover effects while all other parameters (K_1 to k_4 and equilibrium parameters) differed by less than 2% in case of the 2TCM and less than 8% (k_4) in case of the m2TCM.

AUC ratio method and influence of the pre-scan interventions

We additionally estimated specific accumulation with the IF- and model-independent recently applied AUC ratio method (Milicevic Sephton *et al.* 2013, 2015). As concluded from the above IF-dependent analysis, [^{18}F]PSS232 meets all conditions for the suggested AUC ratio method (Introduction): Investigating the data set shown in Fig. 4, θ_2 (1/min) for striatum was 0.13, resulting in an MRT of 7.7 min, less than 1/10 of the scan duration. $1/k_{2,CBref}$ was 0.17 min. Both AUC residues from t_n to $t = \infty$ were thus negligible for the quantification of [^{18}F]PSS232 accumulation. From this we hypothesized that, once constant, AUC_{ROI}/AUC_{CBref} should equal the slope in the Logan reference tissue plot and should get close to $V_{T,ROI}/V_{T,CBref}$.

As shown in Fig. 6(a), AUC ratios of the data of the scan shown in Fig. 4 became approximately constant after 35 min. This was the case for all scans. Figure 6(b) shows the respective Logan reference tissue plot for striatum and hippocampus. All ROIs were further analyzed with the Logan reference tissue method applying $k_{2,CBref} = 5$ (1/min; from Fig. 5 and Table S2). Figure 6C shows the good agreement between the AUC ratio method and the Logan reference tissue method with a slope (AUC ratio/Logan) of 0.97, an intercept of 0.016 (ca 0.5% of maximal AUC_{ROI}/AUC_{Ref}) and r^2 0.992. Bland–Altman analysis revealed a significant but small bias of −0.039 (Figure S9), corresponding to 1.5% of the averaged values for striatum. Figure 7 shows the comparison of $V_{T,ROI}/V_{T,CBref}$, slope of Logan reference tissue plot and AUC_{ROI}/AUC_{Ref} of all analyzed ROIs.

Next, we investigated the influence of the pre-scan intervention to apply an AV-shunt on [^{18}F]PSS232 accumulation by comparing the AUC_{ROI}/AUC_{CBref} ratios of the rats scanned in this study with the ratios recently reported by us for rats in a test–retest experiment without pre-scan intervention (Milicevic Sephton *et al.* 2013, 2015). There was no significant difference between the AUC ratios revealed with the different protocols (Fig. 7). Relative SD of all ROIs and protocols were lower than 7.5%, allowing quantitative comparisons with the AUC ratio method with high statistical power.

Discussion

We evaluated an invasive, a minimally invasive and a non-invasive protocol for quantitative PET in rats with [^{18}F]PSS232, a tracer targeting mGluR5 exclusively as shown in this work with mGluR5 KO rats. While the invasive standard protocol for the recording of the blood TAC via an AV-shunt requires dissection of femoral artery and vein and is, therefore, not appropriate for longitudinal studies, our novel minimally invasive cannulation method is well suited for non-terminal experiments. The cannulation protocol allowed to reduce invasiveness and duration of anesthesia, factors that affect animal physiology and are potential sources for artefacts in quantitative PET. The non-invasive and simple-to-calculate AUC ratio method is ideal for longitudinal studies when one overall parameter for quantitative comparison of receptor density or occupancy between groups or over time is adequate.

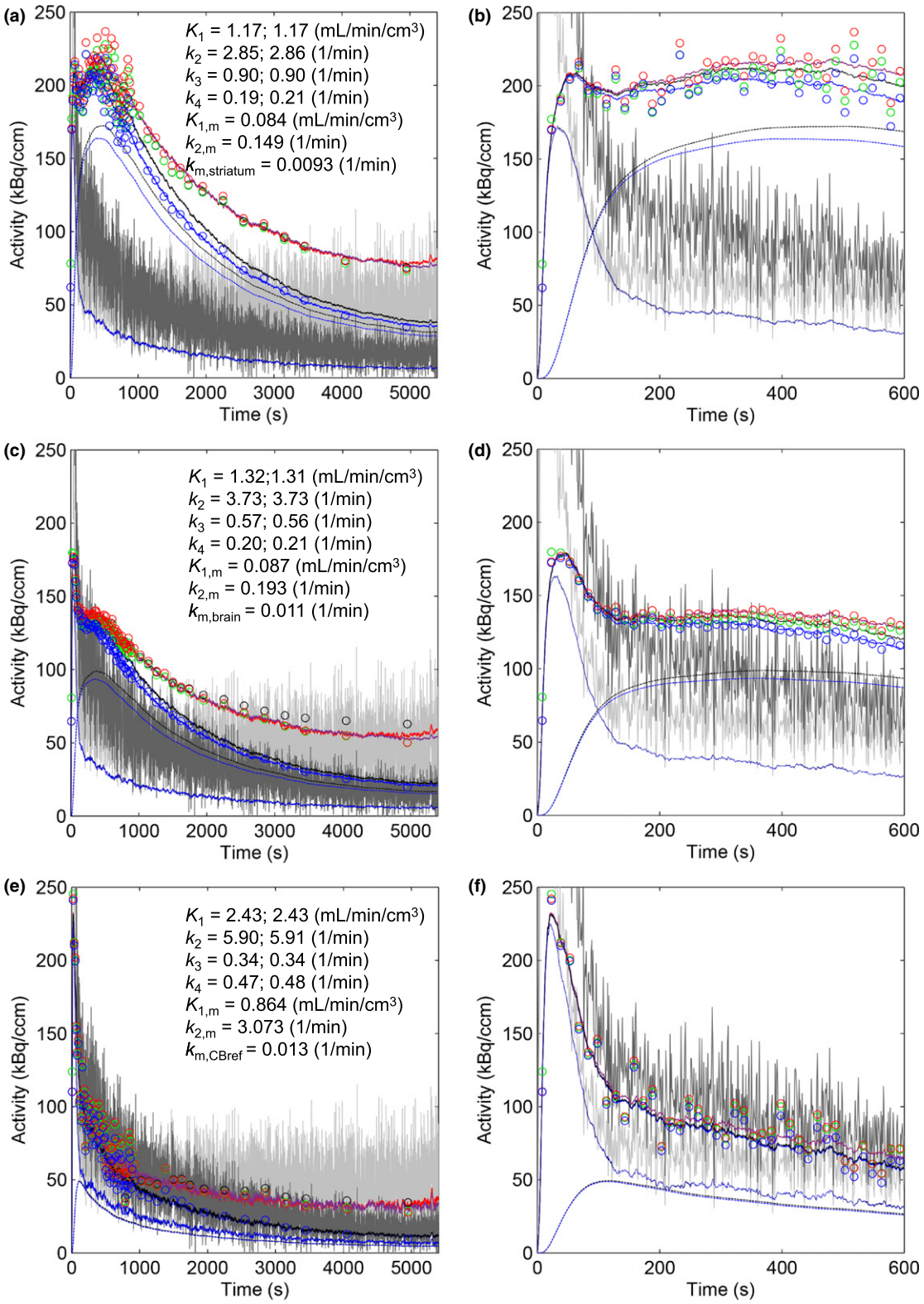
(a)
K_1 = 1.17; 1.17 (mL/min/cm^3)
k_2 = 2.85; 2.86 (1/min)
k_3 = 0.90; 0.90 (1/min)
k_4 = 0.19; 0.21 (1/min)
$K_{1,m}$ = 0.084 (mL/min/cm^3)
$k_{2,m}$ = 0.149 (1/min)
$k_{m,striatum}$ = 0.0093 (1/min)
(b)
(c)
K_1 = 1.32;1.31 (mL/min/cm^3)
k_2 = 3.73; 3.73 (1/min)
k_3 = 0.57; 0.56 (1/min)
k_4 = 0.20; 0.21 (1/min)
$K_{1,m}$ = 0.087 (mL/min/cm^3)
$k_{2,m}$ = 0.193 (1/min)
$k_{m,brain}$ = 0.011 (1/min)
(d)
(e)
K_1 = 2.43; 2.43 (mL/min/cm^3)
k_2 = 5.90; 5.91 (1/min)
k_3 = 0.34; 0.34 (1/min)
k_4 = 0.47; 0.48 (1/min)
$K_{1,m}$ = 0.864 (mL/min/cm^3)
$k_{2,m}$ = 3.073 (1/min)
$k_{m,CBref}$ = 0.013 (1/min)
(f)
Activity (kBq/ccm)
Time (s)

Fig. 4 Kinetic modeling with the standard two-tissue compartment model (2TCM) including a 1TCM for the radiometabolite and the m2TCM, a 2TCM correcting for radiometaboilte(s) in the region of interest (ROI) by $k_{m,ROI}$. (a and b) Striatum; (c and d) whole brain; (e and f) CBref. (b, d, and f) Zoomed into first 10 min. Light gray line, blood radioactivity curve; dark gray line, IF; black symbols, TAC from positron emission tomography (PET) data; green, TAC corrected for spillover from skull ($C_{ROI,spillover\text{-}corr}(t)$); red, further corrected for contribution of blood radioactivity and vascular space in tissue ($C_{ROI,T}(t)$, used for fit); blue, further corrected for parent/total radioactivity in ROI with fit $k_{m,ROI}$ (eqn 18). Magenta line, fit according to standard 2TCM including a 1TCM for the radiometabolite; black solid line, corresponding function for parent tracer ($C_A(t) \boxtimes W$). Red line, fit with the m2TCM (eqn 10); blue solid line, function for parent tracer calculated with the m2TCM ($C_A(t) \boxtimes W$). Broken lines, second tissue compartment: black, 2TCM; blue, m2TCM. Dotted lines, first tissue compartment: black, 2TCM; blue, m2TCM (superimposed). Fit parameters are indicated in (a, c, and d). First values are fit parameters from the standard 2TCM, second values from the m2TCM.

Applying these protocols, we characterized the kinetics of [18F]PSS232 in rat brain in detail. Corrections were required for satisfactory fits with a 2TCM. First, we introduced corrections for spillover from skull because of moderate defluorination of [18F]PSS232 and bone-uptake of [18F]fluoride. Defluorination was predicted for rats but is not expected for humans based on our *in vitro* biotransformation studies with liver microsomes of both species (Milicevic Sephton *et al.* 2013, 2015). Spillover correction was relevant for cortex but was negligible for striatum and hippocampus.

Second, we corrected for radiometabolite distribution to brain by addition of a 1TCM. To reduce complexity from six to five variables, we introduced a model that directly fits the parent/total radioactivity ratio in the individual brain regions (m2TCM), taking advantage of the fact that the ratio of parent tracer to total radioactivity in brain approximated an exponential function, which can be described by a single parameter. The two models revealed similar results, although with a significant 10% bias in k_4 at a < 1% lower sum of squared residuals for the standard model. The standard model thus perfectly describes the kinetics of [18F]PSS232 in rats while the m2TCM may be useful if the analysis with five instead of six variables reveals more reliable results (lower errors).

When omitting correction for spillover, the parameters accounting for radiometabolite distribution were able to

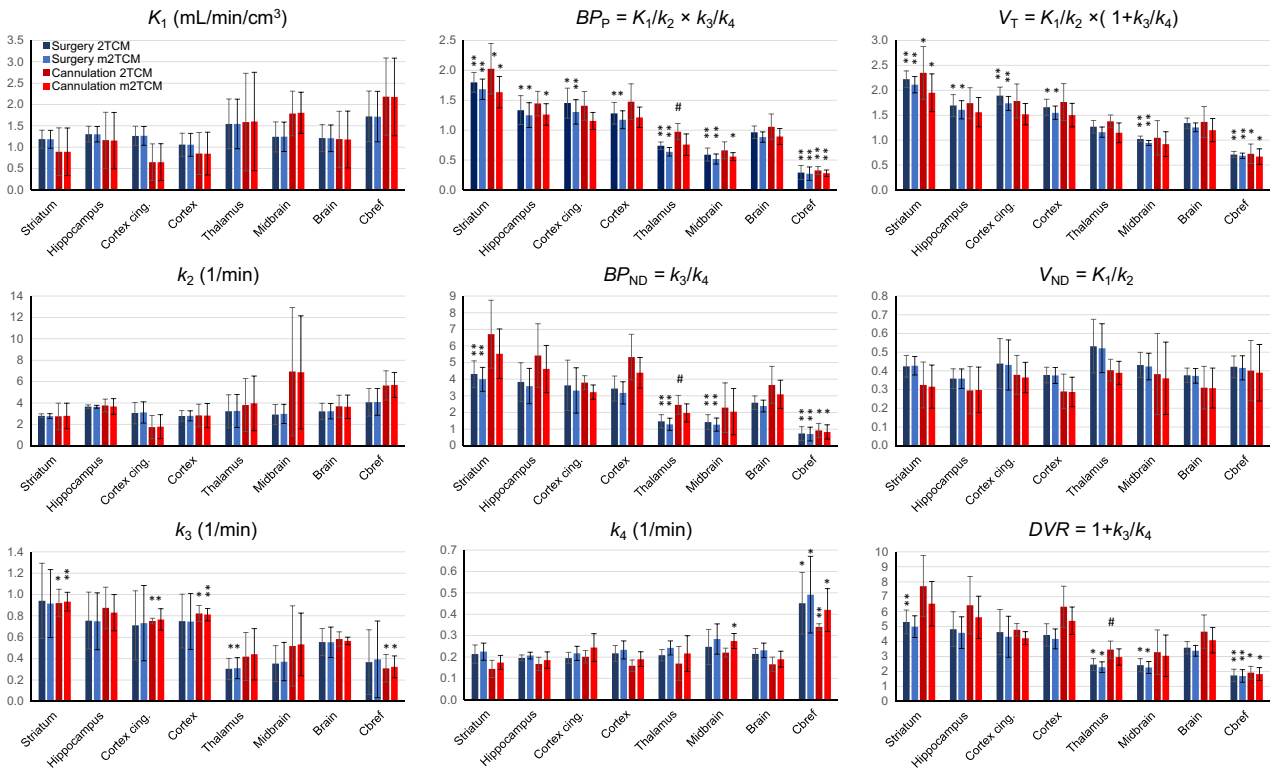

Fig. 5 Fit parameters from the two-tissue compartment model (2TCM) and the m2TCM. The arterio-venous (AV)-shunt for blood radioactivity recording was either applied by surgery ($n = 4$) or cannulation ($n = 3$). Shown are mean values and SD. *, **significantly different from the respective value for whole brain (Brain) at $p < 0.05$ and <0.01, respectively. #significant difference between the surgery and cannulation protocols ($p < 0.05$). Significances for the comparisons with CBref are shown in Table S2.

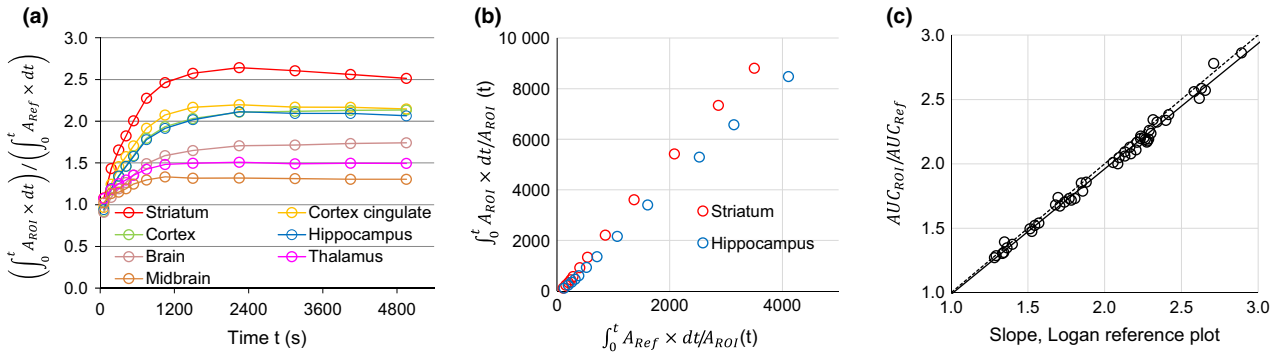

Fig. 6 Evaluation of the area under the curve (AUC) ratio method. (a) Evolution of the AUC_{ROI}/AUC_{CBref} ratios with scan duration. (b) Modified Logan reference tissue plot neglecting correction of the abscissa by addition of $C_{Ref}(t)/C_{ROI}(t) \times 1/k_{2,Ref}$. AUC_{ROI}(75 min)/AUC_{CBref}(75 min) was 2.56 for striatum and 2.09 for hippocampus. The corresponding slopes of the Logan reference tissue plot (b) from $t = 3$ min onwards (second data point) were 2.60 and 2.14. (c) Correlation between the results from the AUC ratio method and the Logan reference method (including correction for $C_{Ref}(t)/C_{ROI}(t) \times 1/k_{2,Ref}$). Solid line, regression line (parameters see text); broken line, line of unity. Rats with surgery and minimally invasive cannulation were included ($n = 7$), all analyzed brain regions.

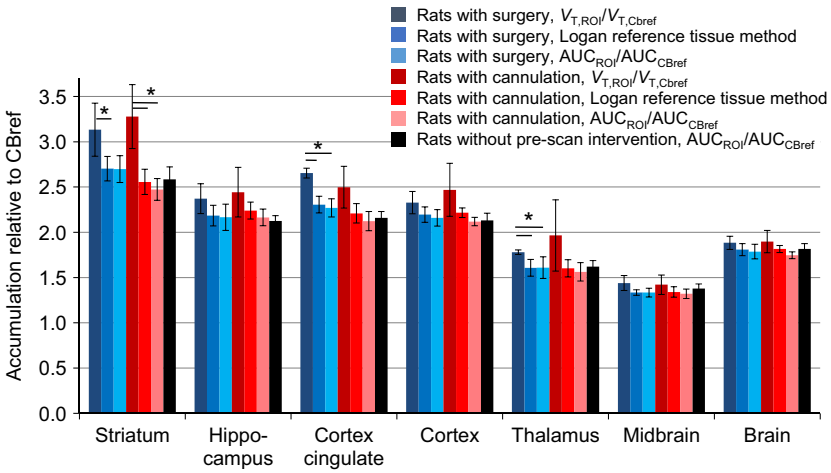

Fig. 7 Accumulation of [^{18}F]PSS232 in rat brain regions relative to CBref as estimated by three models of various complexity. Rats either had a surgery (blue) or a minimally invasive cannulation (red) for the recording of the blood TAC or had no pre-scan intervention [black, data from our recently published test–retest study (Milicevic Sephton *et al.* 2013, 2015))]. Relative accumulation was either estimated from V_T as calculated from K_1 to k_4, requiring an IF (dark blue, dark red), from the Logan reference tissue plot (mid blue, mid red) or the area under the curve (AUC) ratio method (lowest complexity, no parameter assumption required, light blue, light red, black). There were no significant differences between the two reference tissue methods and among the three rat groups (AUC ratio method). V_T ratios were higher than the ratios calculated from the reference tissue methods as V_T but not the other parameters were corrected for the radiometabolite in brain. *significant difference ($p < 0.05$, unpaired) between the V_T ratio and the respective value of the reference tissue method. Inter-group comparisons were only performed for the AUC ratio method.

compensate for this omission. Spillover from bone and radiometabolite distribution to brain may thus be corrected together as they have similar kinetics (both increasing with time), which differs from the kinetics of the parent tracer.

We did not correct the IF for the high fraction of [^{18}F]PSS232 bound to plasma proteins nor for blood cell partitioning. Without these corrections, K_1 in all brain regions was similar to the maximal possible clearance from plasma to brain, namely, the cerebral plasma or blood flow. Typical cerebral blood flow in rat is 1.3–1.9 mL/min/cm^3 (Adam *et al.* 2003; Bos *et al.* 2012). Any correction for plasma protein binding or blood cell partitioning would have resulted in K_1 values higher than plasma or even blood flow. We, therefore, concluded that equilibria between free and bound tracer are much more quickly achieved than the flow-limited transfer across the blood–brain barrier, with the consequence that binding to plasma proteins and blood cells have no influence on K_1.

We found similar K_1 values for [18F]PSS232 as recently shown for the structural analog [11C]ABP688 (Wyss *et al.* 2007; Elmenhorst *et al.* 2010). Comparing k_2 of the two tracers, [18F]PSS232 has a significantly shorter half-life (higher k_2) for the passage back from brain to plasma than [11C]ABP688 (Elmenhorst *et al.* 2010), resulting in a lower V_{ND} of 0.3–0.4 L/kg. The rate constants of receptor interaction (k_3, k_4) were both significantly higher for [18F]PSS232, whereas the ratio k_3/k_4, determining BP_{ND} was similar for the two tracers. For striatum, BP_{ND} was about 4 for [11C]ABP688 (Elmenhorst *et al.* 2010) and 4.3 ± 0.8 for [18F]PSS232 (2TCM, surgery). As a consequence of the lower V_{ND} of [18F]PSS232, V_T values were lower for this tracer than for [11C]ABP688. V_T for striatum equaled 8.5 ± 2.3 for [11C]ABP688 (Elmenhorst *et al.* 2010) and 2.2 ± 0.2 for [18F]PSS232.

Assuming similar distribution between plasma and brain as between plasma and other tissues, V_{ND} corresponds to the pharmacokinetic volume of distribution at equilibrium (V_D) as estimated by dividing the applied radioactivity dose by the back-extrapolated radioactivity concentration at $t = 0$ of the terminal phase of the IF. V_D estimated from Fig. 3(b) is ~ 0.2 L per kg body weight, in the range of V_{ND}. In general, V_D can be estimated as $(0.1 \times \log D + 1) \times f_u$ (Ritschel and Hammer 1980). The so-predicted V_D of [18F]PSS232 and [11C]ABP688 are 0.3 and 3.6 L/kg, respectively, with log D 2.0 and 2.4 and f_u 0.03 and 0.14, respectively (Ametamey *et al.* 2006; Elmenhorst *et al.* 2010; Milicevic Sephton *et al.* 2013). The higher plasma protein binding and lower log D of [18F]PSS232 are thus reducing non-specific tracer accumulation in brain without a loss in specific accumulation compared to [11C]ABP688. However, in rat brain, a polar radiometabolite of [18F]PSS232 substantially increases background radioactivity. This is not expected in humans based on metabolism studies with liver microsomes of both species (Milicevic Sephton *et al.* 2015).

To avoid recording of a blood TAC and to exclude any bias from model-related assumptions or an auxiliary parameter, we applied an AUC ratio method for [18F]PSS232, which produced reproducible results in a previous test–retest study (Milicevic Sephton *et al.* 2013, 2015). Here, we evaluated it in more detail and theoretical considerations as well as experimental comparison showed a good agreement with the Logan reference tissue method, with a significant but negligible bias. The high value of k_2 and the low radioactivity in brain toward the end of the scan are prerequisites for the good agreement. With respect to spillover and radiometabolite distribution, the AUC ratio method is subject to the same bias as the Logan reference tissue method (Logan *et al.* 1996; Ichise *et al.* 2001). The AUC ratio method bears the advantage that no further data transformation and auxiliary parameter are required for analysis. The AUC is directly copied to the clipboard from the PMOD software when generating TACs.

No significant difference was observed between the AUC_{ROI}/AUC_{CBref} ratios of this study, where rats underwent surgery or cannulation, and those of our previous study without any pre-scan intervention (Milicevic Sephton *et al.* 2013, 2015). This excludes a major effect of the anesthesia duration and pre-scan interventions on the PET results with [18F]PSS232.

Our study has some limitations. First, our small group sizes did not allow to compare the two AV-shunt methods in terms of inter-individual variability. Only future studies will show whether one method is more robust than the other. Second, we did not retest the rats with cannulation to prove that cannulation is repeatedly possible. Based on our experience with cannulation for other purposes, we know that repeatability depends on the damage caused by former cannulations. The method thus requires some practice before longitudinal studies with repeated cannulations are envisaged. A third issue is the radiometabolite analysis by TLC. We cannot exclude that TLC spots contained more than one radiolabeled compound. However, the perfect fits with the 2TCM extended for one radiometabolite are in agreement with our assumption of a single (polar) radiometabolite.

In conclusion, PET kinetic modeling in rats with a highly time-resolved IF is achievable with a minimally invasive protocol. We extended the 2TCM by one variable to correct for radiometabolites in individual ROIs and suggest this model, m2TCM, as an alternative to the 2TCM for full kinetic analysis with [18F]PSS232 in rats if the corresponding reduction in variables increases fit reliability. If absolute quantification is not required, the simple, model-independent AUC ratio method and the Logan reference tissue plot reveal robust results for quantitative PET with [18F]PSS232 in rats. [18F]PSS232 is a promising radioligand for quantitative mGluR5 imaging in rat and presumably human brain.

Acknowledgments and conflict of interest disclosure

We thank Martina Dragic, Gloria Pla, Annette Krämer, and Susanne Geistlich for [18F]PSS232 radiosynthesis. Mathworks support team and 'eddie' are acknowledged for the mod_nlinfit.m script allowing to fix fit parameters implemented in our Matlab code. SMS, LM, RS, SMA, and SDK are inventors on the patent 'Fluorinated pyridyl-acetylene derivatives as tracers', including PSS232 (WO 2013182411 A1). The authors have otherwise no conflicts of interest to declare.

All experiments were conducted in compliance with the ARRIVE guidelines.

Supporting information

Additional supporting information may be found in the online version of this article at the publisher's web-site:

Data S1. MATLAB script for modeling with the 2TCM and m2TCM.

Appendix S1. Supplementary Materials and methods.

Figure S1. The standard 2TCM and the modified m2TCM for PET kinetic modeling with a tracer with radiometabolite(s).

Figure S2. Regions of interest for [^{18}F]PSS232 PET kinetic analysis and spillover correction.

Figure S3. [^{18}F]PSS232 TACs of brain regions and skull of an mGluR5 KO rat.

Figure S4. [^{18}F]FDG fit parameters comparing the novel minimally invasive AV-shunt protocol (red) with the standard surgery protocol (gray).

Figure S5. Time–activity curves in striatum (a and b) and CBref (c and d) fitted to a 1TCM (including an additional 1TCM for the radiometaboite) and an m1TCM.

Figure S6. Bland-Altman plots comparing the 2TCM and m2TCM calculation methods for striatum and brain, as indicated.

Figure S7. Kinetic parameters of the radiometabolite.

Figure S8. Influence of $k_{m,ROI}$ (1/min) on the kinetic modeling results of striatum.

Figure S9. Bland–Altman comparison of the AUC ratio method and the Logan reference plot method.

Table S1. Factors fspillover,ROI for spillover correction

Table S2. Averaged fit parameters with standard deviations for PET kinetic modeling of [^{18}F]PSS232 with the standard (upper value) and the modified (lower value) two-tissue compartment model (m2TCM) in rats with arteriovenous-shunt surgery (n = 4, S) or cannulation (n = 3, C).

References

Adam J. F., Elleaume H., Le Duc G., Corde S., Charvet A. M., Tropres I., Le Bas J. F. and Esteve F. (2003) Absolute cerebral blood volume and blood flow measurements based on synchrotron radiation quantitative computed tomography. *J. Cereb. Blood Flow Metab.* **23**, 499–512.

Akkus F., Ametamey S. M., Treyer V. *et al.* (2013) Marked global reduction in mGluR5 receptor binding in smokers and ex-smokers determined by [11C]ABP688 positron emission tomography. *Proc. Natl Acad. Sci. USA* **110**, 737–742.

Alf M. F., Marti-Kehl M. I., Schibli R. and Krämer S. D. (2013a) FDG kinetic modeling in small rodent brain PET: optimization of data acquisition and analysis. *EJNMMI Res.* **3**, 61.

Alf M. F., Wyss M. T., Buck A., Weber B., Schibli R. and Krämer S. D. (2013b) Quantification of brain glucose metabolism by 18F-FDG PET with real-time arterial and image-derived input function in mice. *J. Nucl. Med.* **54**, 132–138.

Ametamey S. M., Kessler L. J., Honer M., Wyss M. T., Buck A., Hintermann S., Auberson Y. P., Gasparini F. and Schubiger P. A. (2006) Radiosynthesis and preclinical evaluation of 11C-ABP688 as a probe for imaging the metabotropic glutamate receptor subtype 5. *J. Nucl. Med.* **47**, 698–705.

Backes H., Walberer M., Endepols H., Neumaier B., Graf R., Wienhard K. and Mies G. (2011) Whiskers area as extracerebral reference tissue for quantification of rat brain metabolism using (18)F-FDG PET: application to focal cerebral ischemia. *J. Nucl. Med.* **52**, 1252–1260.

Bos A., Bergmann R., Strobel K., Hofheinz F., Steinbach J. and den Hoff J. (2012) Cerebral blood flow quantification in the rat: a direct comparison of arterial spin labeling MRI with radioactive microsphere PET. *EJNMMI Res.* **2**, 47.

Boylan J. W., Van Liew J. B. and Feig P. U. (1991) Inverse changes in erythroid cell volume and number regulate the hematocrit in newborn genetically hypertensive rats. *Proc. Natl Acad. Sci. USA* **88**, 9848–9852.

Carson R. E. (2003) Tracer kinetic modeling in PET. in *Positron Emission Tomography: Basic Science and Clinical Practice* (Valk P. E., Bailey D. L., Townsend D. W. and Maisey M. N., eds.), pp. 147–179. Springer, London.

Deschwanden A., Karolewicz B., Feyissa A. M. *et al.* (2011) Reduced metabotropic glutamate receptor 5 density in major depression determined by [(11)C]ABP688 PET and postmortem study. *Am. J. Psychiatry* **168**, 727–734.

Elmenhorst D., Minuzzi L., Aliaga A., Rowley J., Massarweh G., Diksic M., Bauer A. and Rosa-Neto P. (2010) In vivo and in vitro validation of reference tissue models for the mGluR(5) ligand [(11)C]ABP688. *J. Cereb. Blood Flow Metab.* **30**, 1538–1549.

Fujita M., Seibyl J. P., Verhoeff N. P. *et al.* (1999) Kinetic and equilibrium analyses of [(123)I]epidepride binding to striatal and extrastriatal dopamine D(2) receptors. *Synapse* **34**, 290–304.

Hefti K., Holst S. C., Sovago J. *et al.* (2013) Increased metabotropic glutamate receptor subtype 5 availability in human brain after one night without sleep. *Biol. Psychiatry* **73**, 161–168.

Hulka L. M., Treyer V., Scheidegger M. *et al.* (2014) Smoking but not cocaine use is associated with lower cerebral metabotropic glutamate receptor 5 density in humans. *Mol. Psychiatry* **19**, 625–632.

Ichise M., Meyer J. H. and Yonekura Y. (2001) An introduction to PET and SPECT neuroreceptor quantification models. *J. Nucl. Med.* **42**, 755–763.

Ingvar M., Eriksson L., Rogers G. A., Stone-Elander S. and Widen L. (1991) Rapid feasibility studies of tracers for positron emission tomography: high-resolution PET in small animals with kinetic analysis. *J. Cereb. Blood Flow Metab.* **11**, 926–931.

Innis R. B., Cunningham V. J., Delforge J. *et al.* (2007) Consensus nomenclature for in vivo imaging of reversibly binding radioligands. *J. Cereb. Blood Flow Metab.* **27**, 1533–1539.

Logan J., Fowler J. S., Volkow N. D., Wang G. J., Ding Y. S. and Alexoff D. L. (1996) Distribution volume ratios without blood sampling from graphical analysis of PET data. *J. Cereb. Blood Flow Metab.* **16**, 834–840.

Martinez D., Slifstein M., Nabulsi N. *et al.* (2014) Imaging glutamate homeostasis in cocaine addiction with the metabotropic glutamate receptor 5 positron emission tomography radiotracer [(11)C]ABP688 and magnetic resonance spectroscopy. *Biol. Psychiatry* **75**, 165–171.

Milicevic Sephton S., Mu L., Dragic M., Krämer S. D., Schibli R. and Ametamey S. M. (2013) Synthesis and in vitro evaluation of *E*- and *Z*-geometrical isomers of PSS232 as potential metabotropic glutamate receptors subtype 5 (mGlu5) binders. *Synthesis* **45**, 1877–1885.

Milicevic Sephton S., Müller Herde A., Mu L., Keller C., Rüdisühli S., Auberson Y., Schibli R., Krämer S. D. and Ametamey S. M. (2015) Preclinical evaluation and test–retest studies of ^{18}F-PSS232, a novel radioligand for targeting metabotropic glutamate receptor 5 (mGlu5). *Eur. J. Nucl. Med. Mol. Imaging* **42**, 128–137.

Ritschel W. A. and Hammer G. V. (1980) Prediction of the volume of distribution from in vitro data and use for estimating the absolute extent of absorption. *Int. J. Clin. Pharmacol. Ther. Toxicol.* **18**, 298–316.

Susic D., Mandal A. K. and Kentera D. (1984) Hemodynamic effects of chronic alteration in hematocrit in spontaneously hypertensive rats. *Hypertension* **6**, 262–266.

Weber B., Burger C., Biro P. and Buck A. (2002) A femoral arteriovenous shunt facilitates arterial whole blood sampling in animals. *Eur. J. Nucl. Med. Mol. Imaging* **29**, 319–323.

Wyss M. T., Ametamey S. M., Treyer V. *et al.* (2007) Quantitative evaluation of 11C-ABP688 as PET ligand for the measurement of the metabotropic glutamate receptor subtype 5 using autoradiographic studies and a beta-scintillator. *NeuroImage* **35**, 1086–1092.